The Control Stage of a Modular Multilevel Converter-based Arbitrary Wave shape Generator for Dielectric Testing of High Voltage Grid Assets

Ganeshpure, Dhanashree Ashok ; Soeiro, Thiago B.; Ghaffarian Niasar, Mohamad; Vaessen, Peter

DOI
10.23919/ICPE2023-ECCEAsia54778.2023.10213691

Publication date
2023

Document Version
Final published version

Published in
Proceedings of the 2023 11th International Conference on Power Electronics and ECCE Asia (ICPE 2023 - ECCE Asia)

The Control Stage of a Modular Multilevel Converter-based Arbitrary Wave shape Generator for Dielectric Testing of High Voltage Grid Assets

Dhanashree Ashok Ganeshpure[1], Thiago Batista Soeiro[3], Mohamad Ghaffarian Niasar[1], and Peter Vaessen[1,2]

[1] High Voltage Technology Group, Delft University of Technology Mekelweg 04, 2628 CD, Delft, The Netherlands
[2] KEMA laboratories, Klingelbeeksweg 195, 6812DE, Arnhem, The Netherlands
[3] Power Electronic & EMC Group, University of Twente, Drienerlolaan 5, 7522 NB Enschede, The Netherlands
Author Details: Dhanashree Ashok Ganeshpure (Email: D.A.Ganeshpurer@tudelft.nl)

***Abstract*—A Modular Multilevel Converter (MMC)-based Arbitrary Wave shape Generator (AWG) for High Voltage (HV) testing faces challenges in the control hardware to generate kHz-range high-frequency waveforms. Real Time Simulators (RTS) provide a simple way to implement the control of the MMC-based AWG in the FPGA. One of the commercially available RTS named Typhoon HIL is found to satisfy the small simulation step requirement such as minimum of $200\,\mathrm{ns}$ for generating kHz-range high-frequency waveforms. The performance of Typhoon HIL device is demonstrated with a scaled-down prototype of MMC-based AWG where sinusoidal and other arbitrary waveforms are generated up to $5\,\mathrm{kHz}$ with a THD less than 5 %.**

***Index Terms*—MMC, HV testing, Control Hardware, Real Time Simulators**

I. Introduction

High Voltage (HV) equipment in the electrical power system, such as switchgear, cables, and transformers, are experiencing new electrical stresses due to the rise of Distribution Generation (DG) systems and large-scale renewable energy integration with power electronic converters [1][2]. For this reason, HV equipment must more often endure higher dV/dt stress due to solid-state switching, which can degrade the grid's reliability by weakening the grid's dielectric material. Additionally, conventional HV dielectric test sources, i.e., transformers (cascaded and resonant), impulse generators, and rectifier circuits, face many limitations in terms of flexibility to generate non-standard and complex wave shapes. It is also time-consuming to build customized test setups with multiple sources to generate complex wave shapes. Sometimes, a function generator and an HV amplifier are used to generate arbitrary wave shapes [3]. However, most of the commercially available HV amplifiers have limited current capability and control bandwidth. To address these problems, Modular Multilevel Converter (MMC) topology is proven to be a promising solution for the HV Arbitrary Wave shape Generator (AWG) [4]. The selection of the MMC-based HV AWG can solve the limitations with respect to the higher current capability for high-frequency waveform generation. However, the circuit may require complex control hardware because of the large number of submodules and the requirement for accurate gate pulse generation at high-frequency.

As discussed in [4], a centralized controller offers significant advantages to controlling the MMC-based HV AWG in terms of its simplicity and robustness from flashover during the HV testing. However, this controller requires considerable computational power to generate accurate submodule gate pulses. This can be especially challenging for generating accurate output voltage waveforms with several kHz fundamental frequencies. From this, it is clear that the MMC-based HV AWG needs an FPGA-based controller where the computation step can be lowered to a few hundred nanoseconds. Programming different complex wave shapes in FPGA using VHDL or Verilog can be tedious for the test engineer. Therefore, to simplify the system operation, Real-Time Simulators (RTSs) are chosen to implement the controller of the HV AWG, where the programming for different waveforms can be done using a MATLAB-Simulink interface or similar software. Hence, the main contribution of this article is as follows:

- Study the characteristic of commercially available RTS named Typhoon HIL as a controller for the MMC-based AWG
- Demonstrate the performance of the chosen RTS with a scaled-down prototype of the MMC-based AWG
- Showcase the performance of high-frequency generation as high as $5\,\mathrm{kHz}$ from MMC, which is a significant improvement from generating the $1\,\mathrm{kHz}$ waveform from MMC with the method described in [5]

Section II of this article briefly explains the HV testing application, where the requirements for the MMC-based HV AWG are clarified. Later, Section III describes the schematic of the MMC-based HV AWG with a detailed description of the chosen modulation technique and the control system. Next, Section III summarizes commercially available RTS devices and then goes in-depth about the

system architecture, the minimum possible simulation step, and the highest switching frequency offered by Typhoon HIL. The performance of the selected RTS is showcased with a scaled-down prototype of the MMC-based AWG in Section IV with multiple waveforms. Lastly, Section V concludes the article with future recommendations.

II. HV AWG Application

HV tests are used to determine the dielectric properties of the insulation materials found in grid assets, such as dielectric strength, partial discharge, and dielectric losses. HV insulation properties can be modelled electrically as capacitance [6]. The MMC-based HV AWG is designed to generate a maximum output voltage of $100\,\mathrm{kV}$ for targeting Medium Voltage (MV) class equipment which ranges from $1\,\mathrm{kV}$ to $36\,\mathrm{kV}$ [7]. Please note that the $36\,\mathrm{kV}$ need to be tested for higher voltage than its rated voltage, such as $80\,\mathrm{kV}$ to $100\,\mathrm{kV}$ considering the switching transients occurring in the electric power network [8]. Fig. 1 to 3 shows a basic description of how an MV vacuum circuit breaker, MV distribution transformer, and MV AC cable are tested. The capacitance for above-mentioned MV equipment ranges from $50\,\mathrm{pF}$ to $10\,\mathrm{nF}$ [9][10]. In the EU region, they are currently tested according to the IEC standards [11][12][13][14], mainly including sinusoidal and lightning impulse test waveforms [15]. This paper focuses on generating different periodic waveforms, such as sinusoidal, triangular, and square, which are required in unconventional dielectric testing of different HV material samples [16]. It is important to highlight the main differences between the traditional HVDC transmission application of MMC with the HV AWG application of MMC.

- *The magnitude of power transfer*: For the AWG, the mentioned capacitive load will require a relatively low output current of up to a few amperes. This small current constitutes the reactive power transfer to the equivalent capacitive load required to achieve voltage stresses. Hence the active power requirement is low and represents only the losses within the converter and test object. This is in stark contrast to the HVDC transmission application, where active power flow is in the MW range [17].
- *Test object behaviour*: During an HV test, the breakdown of the test object or flashover is likely. Hence, the test source should supply sufficient energy for the breakdown and protect itself rapidly (in several $\mu\mathrm{s}$ or few ms). In power applications like renewable energy generation and battery energy systems, it could be necessary that the power electronics supply energy for a fault in a coordinated matter that can last a relatively long time (several ms) without disconnection, e.g., Low Voltage Ride Through [18].
- *Operational Frequency*: Generally, a power electronic converter integrated into the grid is used for continuous operation. A test source is used only for a fixed amount of time during working hours. For dielectric tests, the typical test duration varies from 1 minute to 4 hours except for long-term testing and pre-qualification tests.
- *Performance parameter*: The power efficiency of the converter is of utmost importance in energy transmission. However, voltage accuracy is paramount in HV testing. Since there is no intentional active power transfer, the design requirements are centered around output voltage and current, slew rate, and small- and large-signal bandwidth.

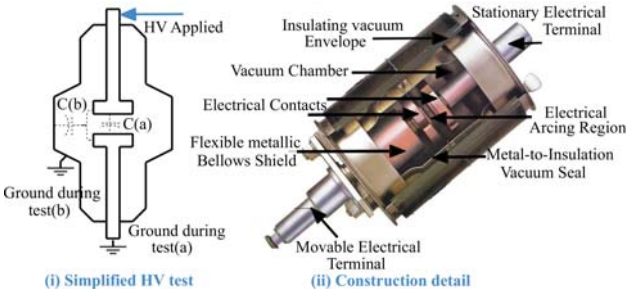

Fig. 1: Vacuum circuit breaker [19]

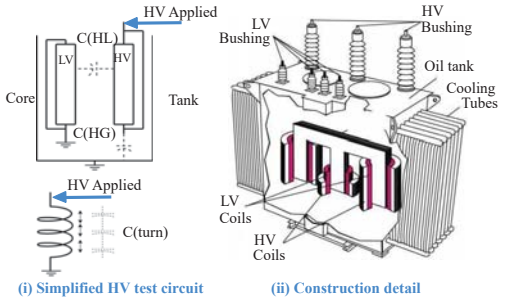

Fig. 2: Distribution Transformer [20]

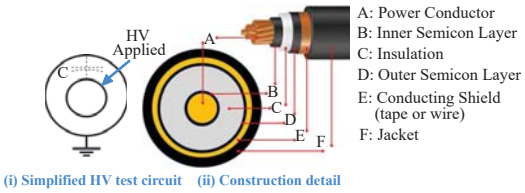

Fig. 3: AC Cable [21]

III. Schematic and Control Of MMC-based HV AWG

Fig. 4(a) shows the schematic of the MMC-based HV test source. It consists of an MMC phase-leg, a split DC source, the AC filter comprising the upper and bottom arm inductance, and a capacitive load representing the equivalent electrical model of the HV equipment under

test [8]. The schematic has a series resistance along with the arm inductance. This is not a stray element but a real passive element to dampen the oscillations generated due to the resonance between the arm inductances and the load capacitance [4]. The complex MMC topology is analysed using its two equivalent circuits, as shown in Fig. 4(b) and Fig. 4(c). The output current circuit in 4(b) dictates the performance of the generated arbitrary voltage waveform since the arm inductance ($\mathrm{L_a}$), arm resistance ($\mathrm{R_a}$), and the load capacitance ($\mathrm{C_{load}}$) act as a low-pass filter with a transfer function, as shown in (1).

$$G_p(s) = \frac{V_a(s)}{V_s(s)} = \frac{2}{L_a C_{load} s^2 + R_a C_{load} s + 2} \quad (1)$$

The abovementioned filter removes unwanted switching harmonics from the switching voltage ($\mathrm{v_s}$). Hence, the correct arm inductance and resistance choice are vital in obtaining highly accurate voltage waveforms. Additionally, the circulating current circuit in Fig. 4(c) helps balance the submodule capacitor voltage by providing the circulating current.

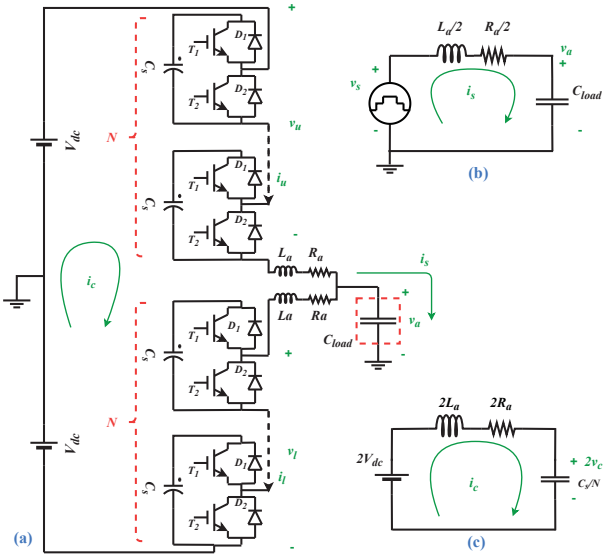

Fig. 4: (a) Schematic of the MMC-based HV AWG (b) Output Current Circuit (c) Circulating Current Circuit

Among the wide variety of modulation techniques, Phase Shift Carrier (PSC) modulation technique is chosen for the HV AWG to obtain highly accurate voltage waveforms [4]. The PSC modulation technique can generate $2\mathrm{N}+1$ number of levels in the switching voltage ($\mathrm{v_s}$) of the MMC by choosing the proper phase shift in the carrier waveforms between Upper Arm (UA) and Lower Arm (LA). For the even number of submodules (N), the phase shift should be π/N and for the odd number of submodules (N), the phase shift should be 0 [22]. The $2\mathrm{N}+1$ levels in the switching voltage shift the switching harmonics far away from the fundamental harmonics, to be precise to $2\mathrm{NF_s}$ [23]. The $\mathrm{F_s}$ is the switching frequency per submodule. This reduces the filtering requirement on $\mathrm{L_a}$ and $\mathrm{R_a}$ and generates accurate voltage waveforms across the load capacitor[4]. The physical implementation of the above-mentioned modulation technique is shown in Fig. 5.

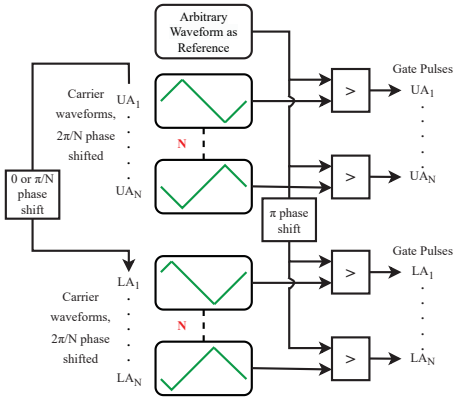

Fig. 5: Block Diagram of the PSC Modulation Techniques

The most significant advantage of the PSC modulation technique is its inherent capability to balance the submodule capacitor voltage [24], and it works well for the HV AWG application due to the negligible steady-state value of circulating current [4]. As per the guidelines discussed in [22], the switching frequency is chosen as a non-integer multiple of the fundamental frequency [22]. However, the sideband frequency $2\mathrm{NF_s}$ should be an integer multiple of the fundamental frequency to balance the submodule capacitor voltages.

IV. Real Time Simulator as a Controller

RTSs are becoming popular in power electronics since they can implement switches and other topologies accurately in the FPGA. Additionally, RTSs are used as a controller to test the power electronics hardware. They can be a suitable solution for MMC since they have many IO ports for controlling many submodules and the availability of an FPGA. Commercially, RTSs are developed by Typhoon HIL, OPAL-RT, dSpace, RT Box and RTDS Simulators. Generally, all these RTSs have a CPU core to process the software interface and multiple CPU and FPGA cores to implement the desired model of a controller, a converter system, or an entire power system. Additionally, FPGA cards are installed at all IO ports to achieve fast communication with external hardware or another RTS. OPAL-RT and dSpace use the MATLAB-Simulink interface, and RTDS uses the RSCAD interface to program the model. However, Typhoon HIL has developed a Python-based software interface to program the CPU and FPGA cores. All the available RTSs have advantages for the particular application.

This article explores the choice of RTS as a controller for the MMC-based HV AWG. The modulation technique presented in Fig. 5 will be implemented in the RTS, and the generated gate pulses will be communicated to the actual hardware via the fibre optic cables. Additionally, the RTS receives the data from the MMC hardware, such as submodule capacitor voltages, arm currents, and hardware health information through a fault signal, for implementing closed-loop control and protecting the MMC hardware. The critical element of the controller implementation is the accuracy of the reference waveform, carrier waveforms, and the generated gate pulses, especially when the reference waveform has a high frequency, such as 5 kHz. The controller needs to operate at a very small simulation step to generate such a high fundamental frequency. Since the Typhoon HIL devices can go to the simulation step of 200 ns [25], this article explores it as a controller for the MMC-based AWG. It includes the theoretical understanding of the RTS architecture, the implementation of the discussed modulation technique, and the effect of the simulation step.

A. Typhoon HIL RTS as a Controller

The Typhoon HIL architecture is shown in Fig. 6, which consists of User CPUs, System CPUs, and FPGA with multiple Standard Processing Cores (SPCs) to process different aspects of the electrical circuits. The System CPUs deal with the low dynamics phenomena such as Voltage RMS calculation or handle the system communication protocol. The User CPUs are under direct user control, and the minimum possible simulation step is 200 ns [25]. Depending upon the complexity of the model, the simulation step needs to be altered so that the implemented model does not have an overrun error. Overrun means the simulation step is insufficient for the RTS to perform all the computations involved within that step [26]. Hence, overruns must be avoided at all costs for the proper operation of the implemented model.

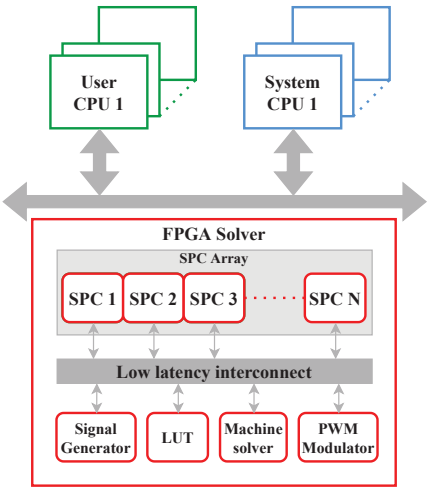

Fig. 6: Typhoon HIL Architecture

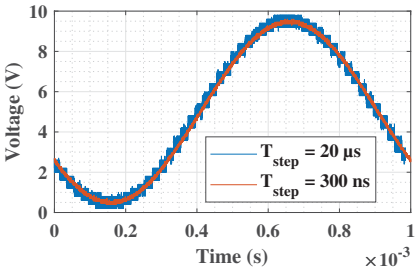

(a) 1 kHz Reference Waveform

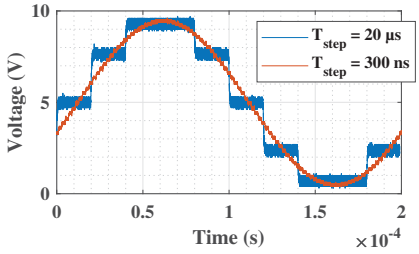

(b) 5 kHz Reference Waveform

Fig. 7: Performance of Typhoon HIL-404 Device for Generating High-Frequency Reference Waveform

The internal PWM modulator block in the FPGA solver can generate accurate gate pulses. This block can configure the carrier waveforms generation in the FPGA for the required switching frequency, the phase shifts, and the dead time. After the generation of these carrier waveforms in the FPGA, they are compared with the reference waveform from the User CPU to generate the gate pulses in the FPGA. The Typhoon HIL devices can generate accurate carrier waveforms with frequencies as high as 500 kHz [27]. It is important to verify if the User CPU can generate accurate reference waveform up to 5 kHz frequency. Hence, the reference waveforms from the HIL-404 device are plotted on an oscilloscope using an analog output port for two different simulation steps. These waveforms are plotted for two frequencies in Fig. 7. From these figures, it is clear that the 20 µs simulation step is not enough to generate a high-frequency reference waveform, and a lower simulation step is required, which is offered by the HIL-404 device.

Moreover, these SPCs in the FPGA solver have dedicated resources for converter modeling, non-ideal switch implementation, etc., as shown in Fig. 6. Different configurations of these SPCs give an optimized performance for a particular application. For example, configuration 3 of the HIL-404 device allows 32 non-ideal switches, which can be implemented in the FPGA, and this number is double when compared to the other SPCs configurations [28].

V. Experimental Setup and Results

The performance of the HIL-404 device as a controller for the MMC-based AWG is demonstrated with a scaled-down prototype. As discussed in Section II, the MMC-based

TABLE I: System Parameters of Down-Scaled MMC Setup

No.	Description	Label	Value
1.	DC link Voltage	V_{dc}	300 V
2.	Output Voltage	V_a	150 V
3.	Number of Submodules	N	2
3.	Modulation Index	m_a	0.9
4.	Submodule Capacitance	C_s	75 µF
5.	Load Capacitor	C_{load}	100 nF
6.	Arm Inductor	L_a	247 µH
7.	Arm Resistor	R_a	90 Ω
8.	Large Signal Bandwidth	$f_{1\%err}$	27.4 kHz
9.	Small Signal Bandwidth	f_{3dB}	49.3 kHz

HV AWG is aimed to be designed for the output voltage of 100 kV with a capacitive load up to 10 nF [4]. However, to test the controller performance, the output voltage is scaled down to 150 V, and it is tested with a higher capacitive load of 100 nF. The arm inductance and arm resistance is designed to obtain the large signal bandwidth of 27.4 kHz and the small signal bandwidth of 49.3 kHz considering the goal of generating 5 kHz waveform. The scaled-down prototype is shown in Fig. 8 with two submodules, and these system parameters of the scaled-down MMC hardware setup are summarized in Table I.

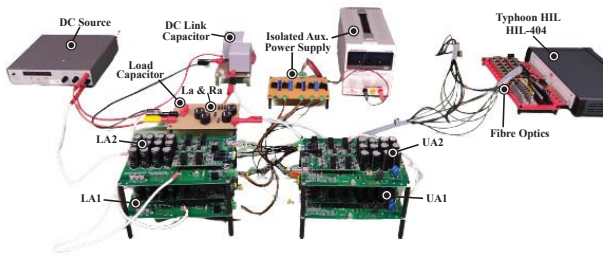

Fig. 8: Scaled-down Hardware Prototype of the MMC-based AWG with Typhoon HIL as a Controller

The performance of the scaled-down prototype is demonstrated with sinusoidal waveforms with different frequencies, such as 1 kHz, 3 kHz, and 5 kHz in Fig. 9 to Fig. 11. These figures show the output characteristics, such as the voltage and current of the MMC-based AWG. Additionally, it is important to verify that the submodule capacitor voltages are well-balanced. Hence, they are displayed for a long duration of 1 s. The submodule capacitor voltages are balanced to a particular average value for all three waveforms and are not deviating away. However, the average value of submodule capacitor voltages is different for higher switching frequency waveforms. Please note that the implemented control system for the MMC-based AWG is an open loop. Generally, the open loop control is sufficient for the MMC-based AWG at lower frequency waveforms, as shown in Fig. 9, with a proper choice of switching frequency, as explained in Section III. Moreover, the quality of the obtained waveforms is shown in the Frequency domain, and the THD values are summarized in Table II, along with the selected value of switching frequencies. It is essential to highlight that the THD of all three sinusoidal waveforms is roughly around 1 %.

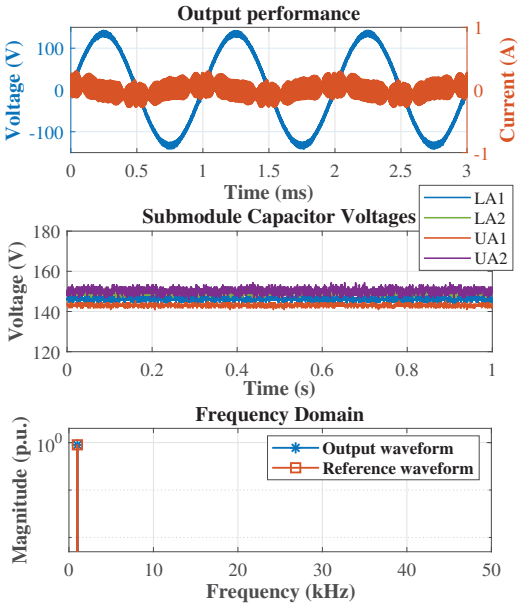

Fig. 9: Sinusoidal waveform with 1 kHz Frequency

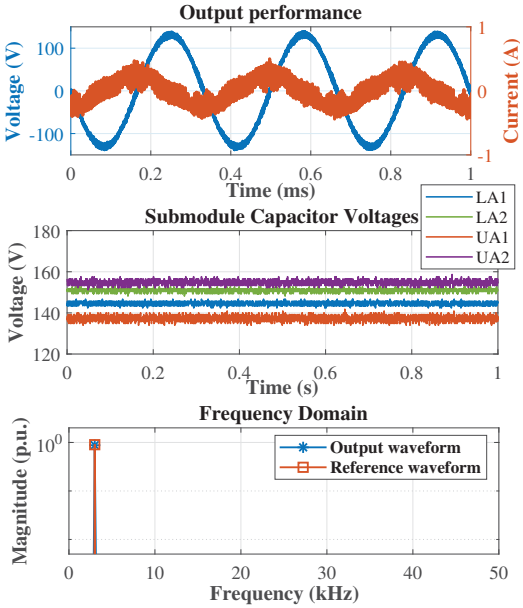

Fig. 10: Sinusoidal waveform with 3 kHz Frequency

Additionally, the performance of the MMC-based AWG is shown with other arbitrary wave shapes, such as triangular and square waveforms. First, the triangular waveform is generated at a high frequency of 5 kHz, as shown in Fig. 12. Apart from the output characteristics and submodule capacitor voltages, frequency domain analysis is performed

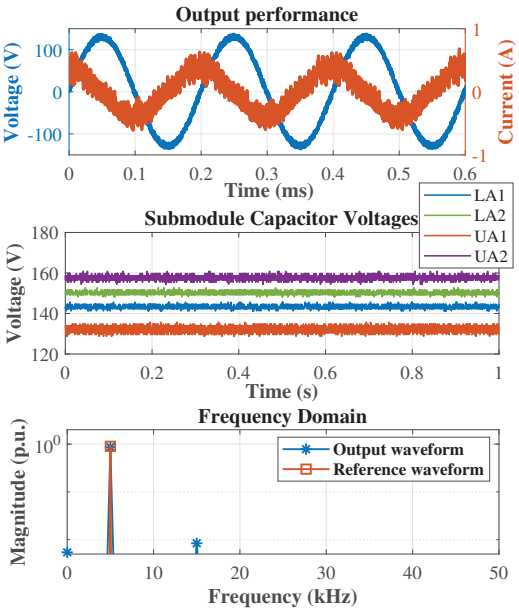

Fig. 11: Sinusoidal waveform with 5 kHz Frequency

TABLE II: Performance of the MMC-based AWG for High Frequency Generation

Waveform	Switching Frequency	THD
Sin with 1 kHz	100.750 kHz	0.4 %
Sin with 3 kHz	144.750 kHz	0.9 %
Sin with 5 kHz	144.750 kHz	1.2 %
Tri with 5 kHz (Filter 1)	144.750 kHz	4.11 %
Tri with 5 kHz (Filter 2)	178.750 kHz	3.62 %
Square with 50 kHz	100.750 kHz	2.01 %

to verify the quality of the waveforms. It is visible that the output waveform is not following the reference waveform well after 5^{th} harmonics (25 kHz) since the designed filter has a large signal bandwidth around the same frequency. Hence, another filter is designed by reducing the load capacitance to more realistic values to 6 nF and increasing the arm resistance to 256 Ω, while the value of arm inductance is kept the same. This filter has large signal bandwidth of 200 kHz and small signal bandwidth of 631 kHz. The effect of the new filter is shown in Fig. 13. Here, the frequency domain harmonics are improved. However, the output voltage waveform has more switching harmonics since the suppressing frequency is farther away with the new filter. This problem can be solved by having higher number of submodules and by having a closed-loop control. Additionally, the submodule capacitor voltages are well balanced since the large-signal bandwidth is far from the fundamental harmonics. The quality of these arbitrary wave shapes is calculated by adapting the definition of THD as follows in (2). The values of THD for two high-frequency waveforms are 4.1 % and 3.6 % with Filter 1 and Filter 2. Due to a larger bandwidth, Filter 2 improves the THD better.

$$THD_{nonsin} = \frac{\sqrt{\sum_{h=0}^{\infty}(V_{h,ref} - V_{h,out})^2}}{V_{1,out}} \tag{2}$$

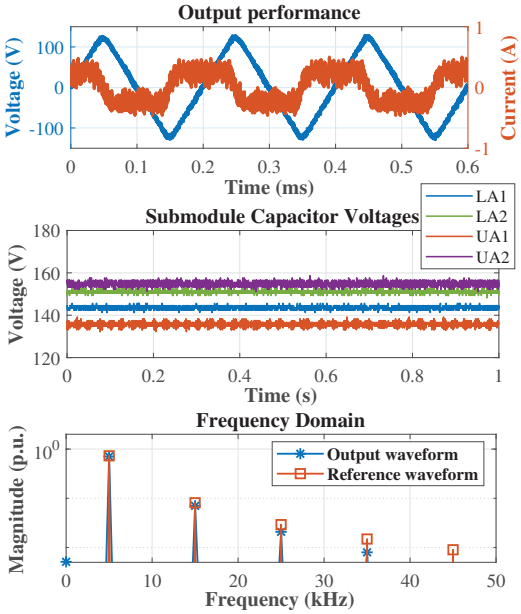

Fig. 12: Triangular waveform with 5 kHz Frequency with Filter 1 and switching frequency of 144.750 kHz

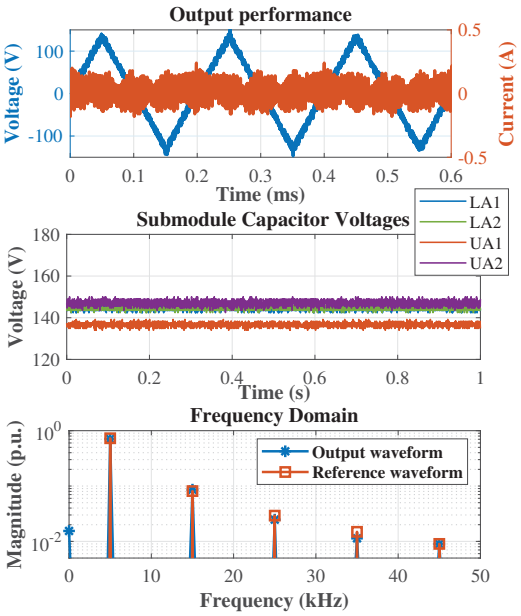

Fig. 13: Triangular waveform with 5 kHz Frequency with Filter 2 and switching frequency of 178.750 kHz

Apart from the triangular waveform, a square waveform is generated from the MMC-based AWG since this is a typical voltage stress experienced by the HV equipment in

the inverter-dominated electrical network. The main focus of the test is to check the slope. Hence, a nominal frequency of 50 Hz is chosen with Filter 1 and switching frequency of 100.750 kHz. Its performance is shown in Fig. 14. The submodule capacitor voltages are balanced with a slightly different average value. It could be because of the DC part present in the square waveform. Additionally, the frequency domain waveform resembles the output waveform and the reference waveform, and the obtained THD value is 2.01 %. Moreover, the zoomed version of the slope of the square waveform is shown in Fig. 15. Based on the output current circuit, the slope can be theoretically calculated as five times the $R_a C_{load}$ time constant. The slope of 20 µs is obtained, which can be further improved with a more realistic load capacitances and a smaller value of arm inductor.

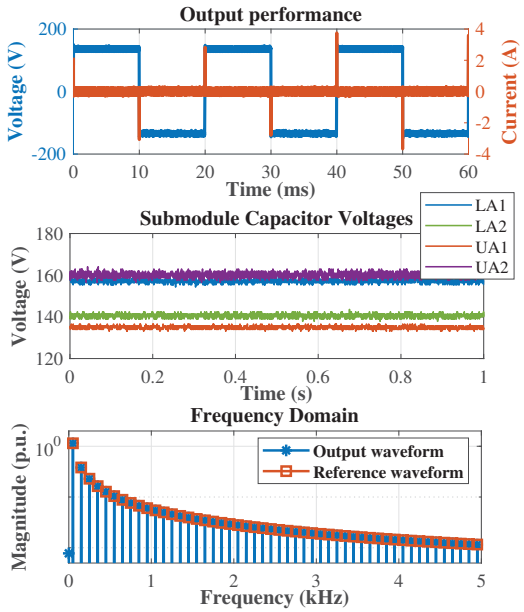

Fig. 14: Square Waveform with 50 Hz frequency

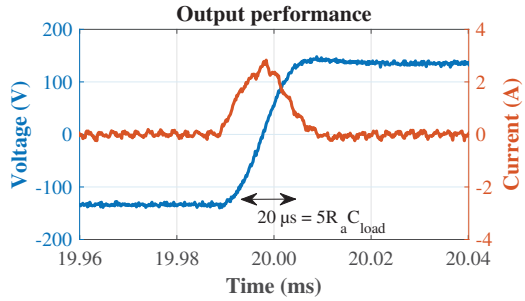

Fig. 15: Zoomed version of Square Waveform with 50 Hz frequency

In summary, the MMC-based AWG can generate arbitrary wave shapes at high-frequency with THD < 5 %, the industrial standard for voltage quality [29]. Apart from the controller accuracy, other factors such as the filter design (R_a, L_a, C_{load}), choice of switching frequency, and the number of submodules play a crucial role in obtaining a good quality of voltage waveform. A closed-loop control would result in a more accurate waveform.

VI. Conclusion and Further Recommendations

This article presents an innovative application of MMC-based HV AWG controlled by an RTS. One of the commercially available RTS, named Typhoon HIL, satisfies the criteria of the small simulation step and can generate accurate high-frequency reference waveforms, carrier waveforms, and gate pulses. Its performance is demonstrated on a scaled-down prototype of the MMC-based AWG with two submodules per arm, and arbitrary high-frequency waveforms up to 5 kHz are generated accurately with THD less than 5 %. To conclude, the MMC-based AWG can fulfill the future HV test requirements on HV grid assets by selecting Typhoon HIL device as a controller and correctly choosing MMC system parameters.

Acknowledgment

The authors would like to thank KEMA Laboratories, Arnhem, and the Dutch TKI Urban Energy Program for their financial support for this work. Additionally, the authors would like to thank Nitish Kulkarni and Sandhyaa Subramaniam for their dedicated work on understanding Real Time Simulators in detail.

References

[1] T. Bengtsson, F. Dijkhuizen, L. Ming, F. Sahlen, L. Liljestrand, D. Bormann, R. Papazyan, and M. Dahlgren, "Repetitive fast voltage stresses-causes and effects," *IEEE Electrical Insulation Magazine*, vol. 25, no. 4, pp. 26–39, 2009.

[2] S. Mukherjee, Y.-J. Häfner, S. Nyberg, and M. Saltzer, "Cable overvoltage for mmc based vsc hvdc system: Interaction with converters," *CIGRE India Journal*, vol. 7, no. 2, pp. 18–23, 2018.

[3] "Advanced Energy - High Voltage Power Amplifier Products." https://www.advancedenergy.com/products/high-voltage-products/high-voltage-amplifiers/. [Accesed on 13 December 2020].

[4] D. A. Ganeshpure, T. B. Soeiro, M. G. Niasar, P. Vaessen, and P. Bauer, "Design trade-offs of modular multilevel converter-based arbitrary wave shape generator for conventional and unconventional high voltage testing," *IEEE Open Journal of the Industrial Electronics Society*, vol. 2, pp. 584–605, 2021.

[5] J. Pan, Z. Ke, M. Al Sabbagh, H. Li, K. A. Potty, W. Perdikakis, R. Na, J. Zhang, J. Wang, and L. Xu, "7-kv 1-mva sic-based modular multilevel converter prototype for medium-voltage electric machine drives," *IEEE Transactions on Power Electronics*, vol. 35, no. 10, pp. 10137–10149, 2020.

[6] F. H. Kreuger, "Industrial High Voltage Volume I: 1. Electric fields, 2. Dielectrics, 3. Constructions," 1991.

[7] "NEN-EN 50160, Voltage characteristics of electricity supplied by public electricity networks," 2010.

[8] F. H. Kreuger, "Industrial High Voltage Volume II: 4. Co-ordinating, 5. Measuring, 6. Testing," 1992.

[9] "Internal test reports, KEMA Laboratories, Arnhem, Netherlands." Confidential.

[10] A. Greenwood, "Electrical transients in power systems," 1991.

[11] "IEC 62271-1, High-voltage switchgear and controlgear – part 1: Common specifications for ac switchgear and controlgear," 2017.

[12] "IEC 60076-1, Power transformers – part 1: General," 2011.

[13] "IEC 60076-3, Power transformers – part 3: Insulation levels, dielectric tests and external clearances in air," 2013.
[14] "IEC 60502-2, Power cables with extruded insulation and their accessories for rated voltages from 1 kv (um = 1,2 kv) up to 30 kv (um = 36 kv) – part 2: Cables for rated voltages from 6 kv (um = 7,2 kv) up to 30 kv (um = 36 kv)," 2014.
[15] "IEC 60060-1, High-voltage test techniques - part 1: General definitions and test requirements," 2011.
[16] X. Wang, *Partial discharge analysis at arbitrary voltage waveform stimulus*. PhD thesis, KTH Royal Institute of Technology, 2012.
[17] E. KONTOS, *Protection of Multiterminal HVDC Grids based on Modular Multilevel Converters*. PhD thesis, Delft University of Technology, 2018.
[18] P. N. Joshi and S. Dadaso Patil, "Improving low voltage ride through capabilities of grid connected residential solar pv system using reactive power injection strategies," in *2017 International Conference on Technological Advancements in Power and Energy (TAP Energy)*, pp. 1–3, 2017.
[19] "4 Methods of Medium-Voltage Circuit Breaker Design." https://testguy.net/content/245-4-Methods-of-Medium-Voltage-Breaker-Design. [Accesed on 24 April 2021].
[20] "Construction of Power Transformer." http://eee-resetsg.blogspot.com/2016/02/construction-of-power-transformer.html. [Accesed on 31 May 2021].
[21] A. Shekhar, X. Feng, A. Gattozzi, R. Hebner, D. Wardell, S. Strank, A. Rodrigo-Mor, L. Ramírez-Elizondo, and P. Bauer, "Impact of dc voltage enhancement on partial discharges in medium voltage cables—an empirical study with defects at semicon-dielectric interface," *Energies*, vol. 10, no. 12, p. 1968, 2017.
[22] K. Ilves, L. Harnefors, S. Norrga, and H.-P. Nee, "Analysis and operation of modular multilevel converters with phase-shifted carrier pwm," in *2013 IEEE Energy Conversion Congress and Exposition*, pp. 396–403, 2013.
[23] K. Sharifabadi, L. Harnefors, H.-P. Nee, S. Norrga, and R. Teodorescu, *Design, control, and application of modular multilevel converters for HVDC transmission systems*. John Wiley & Sons, 2016.
[24] W. van der Merwe, P. Hokayem, and L. Stepanova, "Analysis of the n -cell single phase mmc natural balancing mechanism," *IEEE Journal of Emerging and Selected Topics in Power Electronics*, vol. 2, no. 4, pp. 1149–1158, 2014.
[25] "Typhoon HILL Specifications." https://www.typhoon-hil.com/. [Accesed on 7 March 2023].
[26] S. Subramaniam, "Implementation of control for mmc-based arbitrary wave shape generator in the opal-rt simulator," 2021.
[27] "PWM Modulator." https://www.typhoon-hil.com/documentation/typhoon-hil-software-manual/References/pwm_modulator.html?hl=pwm%2Cmodulatore. [Accesed on 7 March 2023].
[28] "Typhoon HILL SPCs Details." https://ticket.typhoon-hil.com/kb/faq.php?id=184. [Accesed on 7 March 2023].
[29] "IEC 61000-2-4: Electromagnetic compatibility (EMC) - part 4: Compatibility levels in industrial plants for low-frequency conducted disturbances," 2017.